AGU PUBLICATIONS

JGR

Journal of Geophysical Research: Atmospheres

RESEARCH ARTICLE

10.1002/2013JD020877

Key Points:
- High-resolution climate simulations important for local-scale interactions
- Bioenergy cools and moistens projected future climate in summer
- Importance of agricultural practices

Supporting Information:
- Readme
- Figure S1

Correspondence to:
M. H. Tölle,
mschlue@gwdg.de

Citation:
Tölle, M. H., O. Gutjahr, G. Busch, and J. C. Thiele (2014), Increasing bioenergy production on arable land: Does the regional and local climate respond? Germany as a case study, *J. Geophys. Res. Atmos.*, *119*, 2711–2724, doi:10.1002/2013JD020877.

Received 27 SEP 2013
Accepted 11 FEB 2014
Accepted article online 14 FEB 2014
Published online 18 MAR 2014

Increasing bioenergy production on arable land: Does the regional and local climate respond? Germany as a case study

Merja H. Tölle[1], Oliver Gutjahr[2], Gerald Busch[3], and Jan C. Thiele[4]

[1]Department of Bioclimatology, Büsgeninstitut, Georg-August-Universität Göttingen, Göttingen, Germany, [2]Faculty of Geography/Geosciences, Department of Environmental Meteorology, University of Trier, Trier, Germany, [3]Bureau for Applied Landscape Ecology and Scenario Analysis, Göttingen, Germany, [4]Department of Ecoinformatics, Biometrics, and Forest Growth, Büsgeninstitut, Georg-August-Universität Göttingen, Göttingen, Germany

Abstract The extent and magnitude of land cover change effect on local and regional future climate during the vegetation period due to different forms of bioenergy plants are quantified for extreme temperatures and energy fluxes. Furthermore, we vary the spatial extent of plant allocation on arable land and simulate alternative availability of transpiration water to mimic both rainfed agriculture and irrigation. We perform climate simulations down to 1 km scale for 1970-1975 C20 and 2070-2075 A1B over Germany with Consortium for Small-Scale Modeling in Climate Mode. Here an impact analysis indicates a strong local influence due to land cover changes. The regional effect is decreased by two thirds of the magnitude of the local-scale impact. The changes are largest locally for irrigated poplar with decreasing maximum temperatures by 1°C in summer months and increasing specific humidity by 0.15 g kg^{-1}. The increased evapotranspiration may result in more precipitation. The increase of surface radiative fluxes R_{net} due to changes in latent and sensible heat is estimated by 5 W m^{-2} locally. Moreover, increases in the surface latent heat flux cause strong local evaporative cooling in the summer months, whereas the associated regional cooling effect is pronounced by increases in cloud cover. The changes on a regional scale are marginal and not significant. Increasing bioenergy production on arable land may result in local temperature changes but not in substantial regional climate change in Germany. We show the effect of agricultural practices during climate transitions in spring and fall.

1. Introduction

Climate change mitigation and adaption actions encompass CO_2 reduction [*Intergovernmental Panel on Climate Change* (*IPCC*), 2007]. Achieving this, the European Union (EU) enacted to increase the percentage of energy from renewable sources like solar, wind, and bioenergy to 20% of the total energy consumption by 2020 [*EU*, 2009]. Involved land use and land cover change (LULCC) due to bioenergy production may thus increase in Europe in the future. *Özdemir et al.* [2009] estimated an increase in the land area dedicated to energy crops of ~21 million ha in the EU. This in turn can trigger climate changes especially on local and regional scales.

Previous LULCC studies used mainly global or regional climate models with coarse resolution to evaluate potential biosphere-atmosphere effects with conflicting results. First, studies focused on land cover changes concerning a complete change mostly from forest to grassland by clearance for pasture on a global scale [*Turner et al.*, 1994]. This resulted in a cooling in the surface climate [*Oleson et al.*, 2004; *Bonan*, 2001]. In addition, *Feddema* [2005] argued that agricultural expansion resulted in cooling and a decrease of the average daily mean temperature range in future climates. Whereas, *Douville et al.* [2000] pointed out that high uncertainties exist on regional scale as expressed in the high sensitivity of the climate in European summertime. *Li and Mölders* [2008] found opposing responses to land cover change and climate warming in different regional areas. They stressed the local effects of land cover change and assessed the resulting impacts to be of regional importance rather than affecting large-scale cycles. However, studies like *Gedney and Valdes* [2000], *Swann et al.* [2012], and *Jones et al.* [2013] demonstrated also large-scale circulation changes and hydrological teleconnections associated with large-scale land cover changes.

Extreme events such as heat waves, droughts, or floods will likely increase in frequency and intensity in the future based on projections of global and regional climate models [*Meehl et al.*, 2005; *Tölle et al.*, 2013;

Coumou and Robinson, 2013]. *Zaitchik et al.* [2006] found a heat dampening effect of forest during the heat wave 2003 in France based on satellite data. It is believed that changes in the surface energy budget are driving the evolution of hot summers [*Stegehuis et al.*, 2012]. The authors found that warm summers are preceded by an increase in latent heat flux in early spring. Many studies focus on soil moisture content and climate [e.g., *Seneviratne et al.*, 2010] but miss discussing the possible impact of evapotranspiration from different vegetation types and of agricultural practices. The ease of which energy and matter can be exchanged between the soil and the atmosphere depends on the vegetation density and vegetation type. As such, evapotranspiration is a critical variable in the context of terrestrial vegetation influence on summer heat waves by feeding back the surface energy balance to the hydrological cycle. In addition, the role of irrigation as an important aspect of land management should be further investigated influencing local and regional climate as pointed out by *Boucher et al.* [2004], *Lobell and Bontils* [2008], and *Sacks et al.* [2009].

There are several studies in the U.S. who examined the impact of bioenergy crops on the regional climate, e.g., *Vanloocke et al.* [2010], *Georgescu et al.* [2011], and *Anderson et al.* [2013]. However, the extent and magnitude of LULCC due to renewable energies for regional- and local-scale future climate changes are not yet quantified for Germany. Therefore, we use bioenergy allocation on arable land (for irrigated and nonirrigated poplar and maize) to quantify the future climate effects on local and regional scales in Germany by applying a mesoscale nonhydrostatic regional climate model (COSMO-CLM, Consortium for Small-Scale Modeling in Climate Mode, here abbreviated CCLM, [*Rockel et al.*, 2008]) coupled to a land surface parameterization scheme TERRA-ML [*Schrodin and Heise*, 2002]. We perform climate simulations with a very high horizontal resolution (0.0118°) to account for the local scale. "Local" is referred to the sites which are converted to bioenergy crops, whereas regional means the nonconverted sites. The focus is on future impacts of biophysical changes associated with irrigated poplar, nonirrigated poplar, and maize. Changes of the vegetation parameters lead to changes in parameters controlling the use of available water and energy at the surface which in turn influences the atmospheric variables. Changes in the latter impact the surface fluxes. This in turn can trigger climate changes especially on regional and local scale. In particular, we answer the following questions:

1. How does land use change on arable land influence the simulated climate during the growing season of Germany?
2. How do extreme temperatures and latent and sensible heat change under different climate conditions and vegetation scenarios?

An overview on the regional climate model, its land surface parameterization, and the downscaling method is presented in section 2. Two time slices for the numerical experiments are depicted, 1970–1975 based on the reference scenario C20 and 2070–2075 based on emission scenario A1B of IPCC AR4 [*IPCC*, 2007] using ECHAM5/MPI-OM [*Roeckner et al.*, 2006]. Nine simulations are performed: two reference simulations using the default land surface values of ECOCLIMAP [*Masson et al.*, 2003; *Champeaux et al.*, 2005] for present and future climate, four simulations with extreme modified vegetation cover due to irrigated poplar for present climate, and three others in which suitable arable areas are transformed to irrigated, nonirrigated fast-growing poplar, or maize for future climate. This experimental design is described in section 3. The main results are shown in section 4. Finally, section 5 discusses and outlines the main conclusions of this study.

2. The Regional Climate Model and Downscaling Procedure

Analysis of LULCC are performed with the latest evaluated version (v4.8-clm17) of CCLM. Agricultural fields in Germany are patchy and differentiated in nature and hardly exceed 100 ha. Thus, our target resolution of the simulation domain is 0.0118° $\sim$ 1.3 km. Therefore, our nesting chain begins with the general circulation model ECHAM5/MPI-OM [*Roeckner et al.*, 2006]. The first nest of the CCLM in horizontal resolution of 0.165° ($\sim$ 18 km) was performed by *Hollweg et al.* [2008] (known as consortial runs). These simulations serve as forcing data for our CCLM runs with a resolution of 0.0625° ($\sim$ 7 km), see Table 1 and Figure 1. Finally, these model runs are used to force the CCLM in the target resolution of 0.0118° ($\sim$1.3 km).

The data used are the climate scenarios based on emission scenario A1B (first realization) and the control scenario C20 described in the Special Report on Emission Scenarios [*Nakicneovic et al.*, 2000]. The twentieth century control C20 simulation is taken as a reference of present climate 1970–2000 and the A1B scenario simulation as a possible evolution of future climate 2070–2100. The results of the 0.0625° simulations serve as hourly boundary data for the target resolution (0.0118°) for present climate 1970–1975 based on C20

Table 1. Model Configuration and Downscaling Steps[a]

Model Parameter	First Nesting	Second Nesting
Grid resolution	0.0625° ~ 7 km	0.0118° ~ 1.3 km
# of grid points	254 × 254	375 × 376
Forcing	Consortial simulations CCLM 0.165° ~ 18 km	CCLM 0.0625° ~7 km
Model time step	45 s	12 s
Integration scheme	Runge-Kutta	Runge-Kutta
Atmospheric layers	40	40
Convection scheme	Tiedtke, Graupel	Shallow convection, Graupel
Simulations time	1970–2000	1970–1975
	2070–2100	2070–2075
Greenhouse gas forcing	C20 and A1B IPCC-SRES	Control and emission scenarios (run 1)

[a]The complete 3-D regional climate model consist of two parts: the atmospheric model COSMO 4.8-CLM17 and the land surface scheme TERRA-ML.

and 2070–2075 based on A1B. The difference between the two resolutions is that in the 0.0625° simulations convection is parameterized while in the 0.0118° simulations deep convection is resolved explicitly. The configuration for the convection-resolving climate simulations is adapted from *Knote et al.* [2010]. The domain size of the first nesting covers central Europe (see Figure 1) with 254 × 254 grid points in order to simulate the regional circulation pattern adequately. The size of the target domain of the high-resolution runs covering Central Germany and its very near surroundings with 375 × 376 grid cells is considered to have an adequate dimension to explicitly resolve convection and analyze LULCC while having a high computational cost.

The atmospheric model CCLM is based on simple hydrothermodynamical equations describing a compressible nonhydrostatic flow in a moist atmosphere. It uses a Runge-Kutta time-stepping scheme, the radiation scheme of *Ritter and Geleyn* [1992], and the convection scheme by *Tiedtke* [1989] for convective mass flux parameterization. Biophysical exchange processes between the land surface, atmosphere, and soil in CCLM are contained in the soil-vegetation-atmosphere model TERRA-ML [*Schrodin and Heise*, 2002]. The turbulent exchange between the atmosphere and the underlying surface is modeled by a stability and roughness

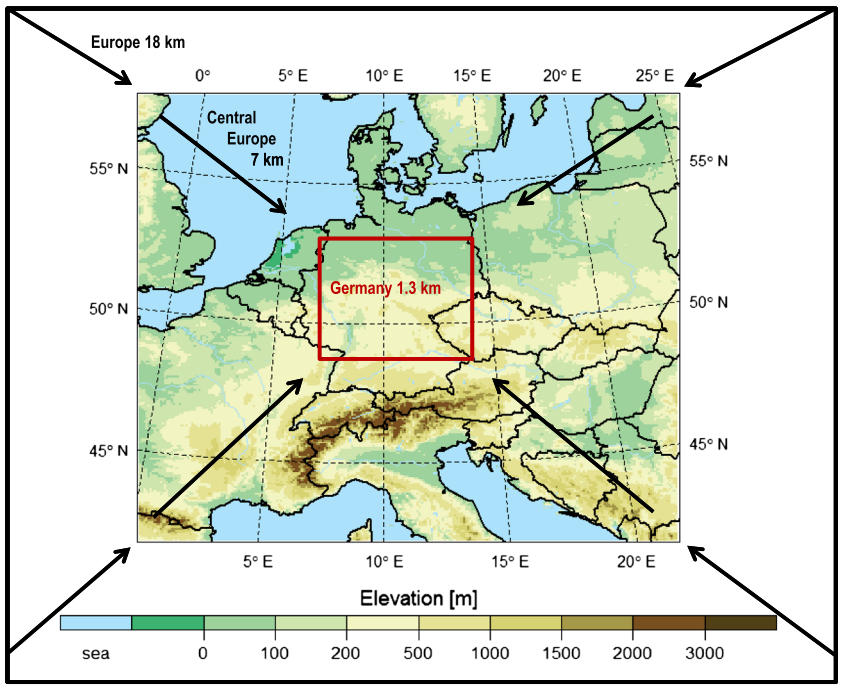

Figure 1. Simulation domain for the two nesting steps. The 7 km simulation domain covers large parts of Europe. The 1.3 km domain covers Central Germany and the northeast of Czechia.

length-dependent surface flux formulation. The hydrologic processes are based on *Doms et al.* [2005] and *Ament and Simmer* [2006]. The variables of the hydrological cycle are determined by using the multisoil layer concept with soil moisture diffusion and soil heat conduction equations for different soil textures as well as frozen soil processes. The Biosphere-Atmosphere Transfer Scheme by *Dickinson et al.* [1993] is implemented for the parameterization of evapotranspiration. The land surface model uses a direct solution of the heat conduction equation. The turbulent exchange is based on the Monin-Obukhov similarity for the constant flux layer. The model considers one vegetation type and soil texture which dominates the area of a grid cell. Each grid cell of TERRA-ML takes one variable of the parameters of vegetation and soil which are spatially distributed based on the data set of ECOCLIMAP [*Masson et al.*, 2003; *Champeaux et al.*, 2005]. The surface fluxes constitute the lower boundary conditions for the atmospheric part of the model.

3. Experimental Design Over Germany

3.1. Land Surface Parameters

The external constant parameter data for the surface boundary of the model are coastlines, lakes, river valleys, land cover types, vegetation parameter, topography, and soil type. The land surface processes are controlled by physical vegetation and soil properties. Parameter values are assigned to each grid cell depending on the land cover type. The allocation of types is derived from a global land cover data set which is available at a 1 km resolution according to the ECOCLIMAP database [*Masson et al.*, 2003; *Champeaux et al.*, 2005]. The parameters are preprocessed for the relevant model resolution according to *Smiatek et al.* [2008]. The model-prescribed vegetation parameters are the leaf area index (LAI), roughness length (z0) due to vegetation, plant cover (PC), and root depth (RD). The parameters LAI, $z0$, and PC are varying on a monthly basis to account for the phenological cycle. Changes in these vegetation parameters lead to changes in variables controlling the use of available water and energy at the surface. The leaf area index in the model influences evapotranspiration through stomatal resistance and defines the size of the canopy precipitation storage capacity. The fractional vegetation cover determines the fraction of a grid cell where vegetation properties affect surface exchange processes. For instance, the turbulent exchange of momentum, energy, and moisture between the surface and the atmosphere is calculated as a function of roughness length. The root depth determines the plant-available soil water capacity.

3.2. Simulations and Suitability Mapping

The model domain with the finest resolution (0.0118°) is chosen for the experimental setup. Energy and mass is transferred in the atmosphere from large scales to small ones and vice versa. Thereby, small-scale perturbations can affect large-scale processes significantly. By increasing the horizontal resolution in a RCM, orography and the land surface heterogeneity are better represented [*Tölle*, 2013]. Therefore, increasing the resolution may be important for both the energy budget of the planetary boundary layer and the atmospheric part of the hydrological cycle.

The following set of simulations is designed to elucidate the response of the regional climate to changed land surface conditions. First, two simulations using the default land surface values of ECOCLIMAP for present (CTR; 1970–1975) and future (CTRA1B; 2070–2075) climates are performed as references for comparison. Second, a performance test is carried out with four simulations using irrigated poplar to get a range of extreme cases for present climate conditions. Therefore, all grid cells within the domain are covered with vegetation values of irrigated poplar by +100%, by +50%, and two by +25% for each simulation (see Figure 4). The grid cell size or patch width is 1.3 km. For the latter of the two +25% experiments the converted patches are 13 km in width.

Third, three future simulations are performed with three vegetation scenarios according to irrigated (iPoplarA1B), nonirrigated poplar (PoplarA1B), and maize (MaizeA1B) for 2070–2075. For that, suitable arable land for bioenergy production is selected and converted to irrigated poplar, nonirrigated poplar, or maize. By combining information from digital soil maps [*Liedekerke et al.*, 2006], the Shuttle Radar Topography Mission digital elevation model [*Farr et al.*, 2007] as well as long-term-average temperature and precipitation from regionalized climate grids [*Müller-Westermaier*, 2004], suitable bioenergy crop sites on arable land [*Keil et al.*, 2011] are determined. All operations take place on a 1 km^2 grid scale. Suitability criteria are depicted from several German studies which refer to practical experience from field plots [*Scholz et al.*, 2006; *Petzold et al.*, 2006; *Röhricht and Buscher*, 2009; *Petzold et al.*, 2010]. Accordingly, 300 mm of precipitation during the vegetation period and annual precipitation of 500 mm are assessed to be the lower limit for short rotation

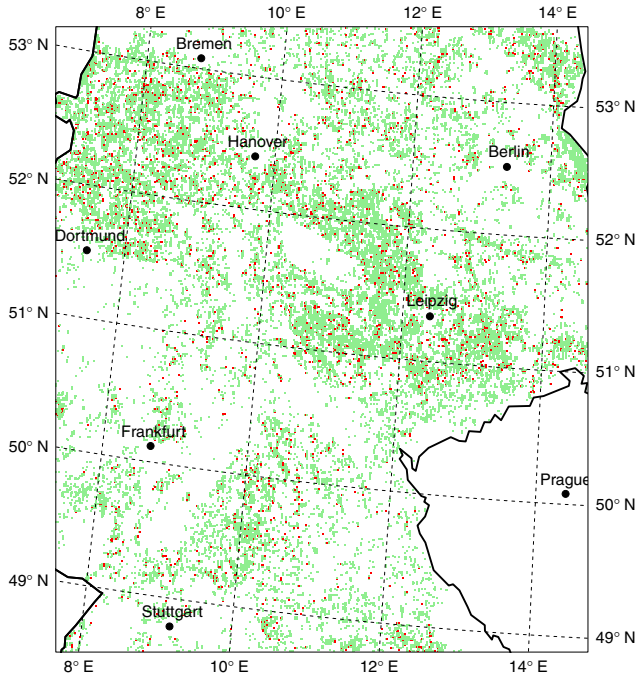

Figure 2. Map of arable areas (green grid cells) and bioenergy areas (red grid cells) of Central Germany for the 1.3 km simulation.

coppice (SRC) suitability. Further, only plots showing an average annual temperature higher than 8°C are selected. Due to harvesting restrictions, sites with steep slopes (>20%) are not considered. Finally, soil and soil water criteria are used to evaluate site suitability. Soils with an available soil water capacity of less than 100 mm imply a high risk of water stress and are appraised as being unsuitable for SRC. The same applies for sites with a groundwater table higher than 50 cm below soil surface or water logging in the upper 50 cm of the soil profile. The criteria are combined by using fuzzy membership functions and calculating with a simple fuzzy "AND" operator [*Busch*, 2012]. Furthermore, the grid cells are evaluated within a 3×3 moving window according to their highest suitability value. With a step size of 3 cells, the moving window "scans" the simulation domain for suitable cells to be converted. Given that arable land accounts for the majority of grid cells within each 3 × 3 moving window (i.e., a minimum of five cells), the most suitable grid cell is selected and mapped. As a result, the ratio of selected cells to be converted ranges between 0% (majority criterion is not met) and 20% (a minimum of five arable cells is present) within each moving window. Following this procedure, the ratio of arable land cells which may be converted to bioenergy fields averages to 9.6% in our study area. The grid cells for bioenergy production are displayed in Figure 2, see the red grid cells. The rest of the arable land cells are displayed in green.

The vegetation parameters (LAI, RD, $z0$, and PC) of the suitable areas are replaced by the characteristics of irrigated, nonirrigated poplar, and maize. The data (LAI, PC, and RD) for the bioenergy plants are derived from a composite of field experiments over different sites in Germany and in particular of the project BEST (bioenergy regions strengthening) [*BEST*, 2011]. The roughness length is approximated after *Monteith and Unsworth* [1990]. The relative seasonal change of the vegetation parameters due to the bioenergy plants compared to the reference values from ECOCLIMAP are shown in Figure 3 as averages over all red grid cells. The values of the vegetation parameters are increased or decreased by a specified amount depending on the bioenergy plant. For iPoplarA1B the values are chosen in such a way that they account for irrigation. The choice of the root depth for iPoplarA1B is motivated by the fact that deeper roots increase plant-available soil water. This allows for increased transpiration rates due to higher LAI. It should be noted that the chosen changes are a strong accentuation that allows us to investigate the interactions and effects between the surface processes and the atmosphere with a larger signal-to-noise ratio. It should not be deemed as a prioritized land use option.

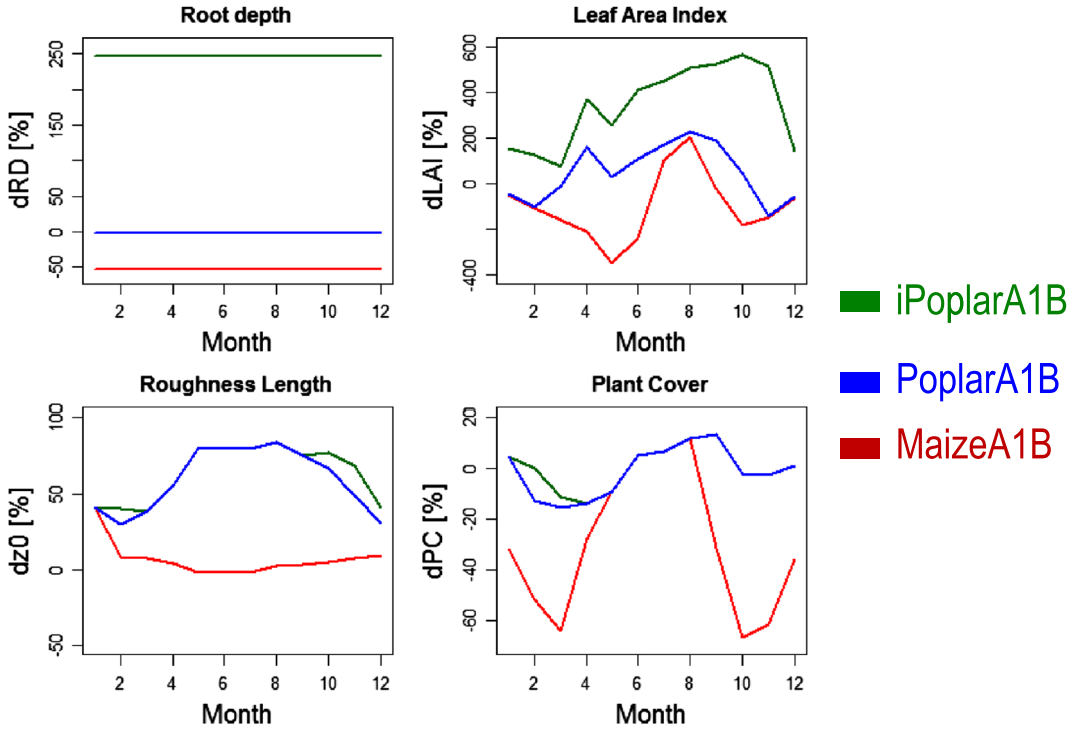

Figure 3. Percental changes of seasonal vegetation parameters compared to the reference of leaf area index, root depth, roughness length, and plant cover averaged over all bioenergy areas.

To elucidate the response of the local and regional climate to changed surface conditions, the reference simulations (CTR and CTRA1B) are compared to the simulations with modified land cover (iPoplarA1B, PoplarA1B, and MaizeA1B). With local we refer to the sites which are converted to bioenergy crops, whereas "regional" means the nonconverted sites. To quantify the magnitude and nature of the climate change signals due to LULCC at a regional scale, the impact of the vegetation scenarios is compared to the impact of global warming.

4. Results

4.1. Range of Extreme Cases

Changes of temperature and precipitation of extreme land cover transformations due to irrigated poplar relative to the reference for present climate (here 1972) are presented in Figure 4. The influence of the vegetation period is strongest in summer (decrease of 0.6°C and increase of 4.5 mm on a monthly basis). The greatest changes appear for 100% land cover change and decline nonlinear with decreasing coverage. The higher LAI in summer along with a deeper root depth are accompanied by a higher evapotranspiration rate and a lower sensible heat flux. This results in a decrease of temperature and an increase of precipitation.

4.2. Impact Ratio

The vegetation impact ratio (vegetation scenario minus CTRA1B divided by vegetation scenario minus CTR) is a measure of the sign and magnitude of the land cover change effect normalized by the size of the total climate change signal. It indicates a strong local negative impact (cooling) during the growing season in the case of irrigated poplar for maximum temperature (see dark blue grid cells in Figure 5a). These grid cells are the suitable areas for bioenergy plants which are shown in Figure 2. On a regional scale this cooling effect is decreased by two thirds (light blue cells in Figure 5a). This negative vegetation-climate influence is less pronounced for nonirrigated poplar (Figure 5b). In the case of maize, equal patterns of positive and negative coupling are indicated (Figure 5c). The effect of conversion is visible directly on the site and its strength depends mainly on the vegetation parameters. For the neighboring grid cells the effect is diminished to a great extent and mixed via advection processes.

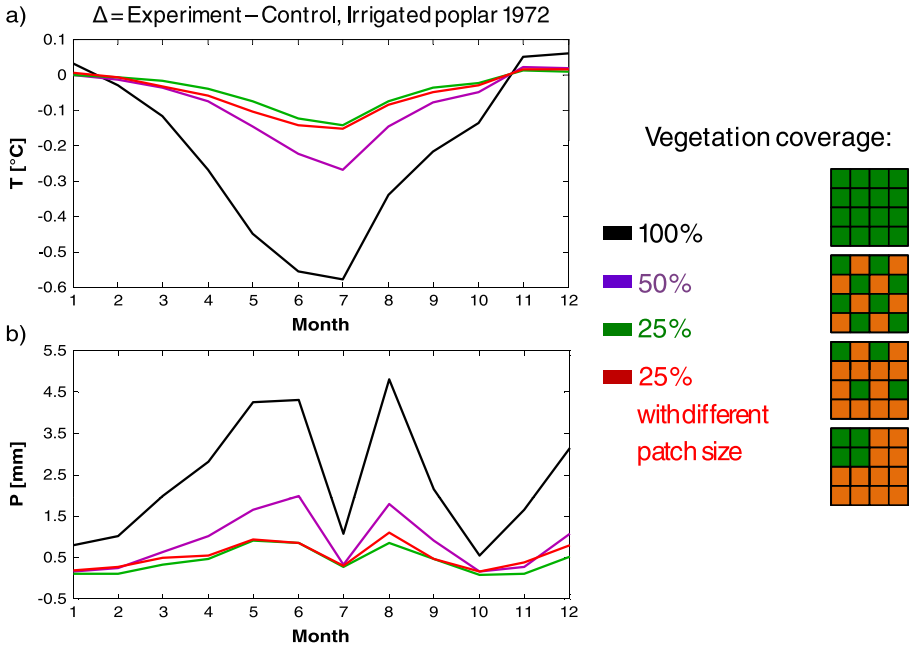

Figure 4. Seasonal changes of (a) temperature and (b) precipitation of extreme land cover transformations due to irrigated poplar relative to the reference for present climate (here 1972). The domain size is covered with vegetation values of irrigated poplar by +100% (black), by +50% (violet), and two by +25% (green). One of the latter has a different patch size (red).

4.3. Local Climate Change Signal of Maximum Temperature

The climate change signal (CCS) as described in *Tölle et al.* [2013] is calculated for each simulation (CTRA1B, iPoplarA1B, PoplarA1B, and MaizeA1B) as the difference between the projected maximum temperature per vegetation period (May to September) averaged over the future period (2071–2075) for each grid cell and the control period (1971–1975) representing the averaged maximum temperature of the reference simulation. The CCS for the growing season of each experiment over the domain is shown as a probability function based on kernel density estimation in Figure 6. The model results show that projected reference extreme temperatures over Germany increased significantly during the vegetation period (Figure 6) by 3.6°C on average. This is broadly consistent with previous estimates [*Jacob et al.*, 2012] based on the same future climate model scenario. Temperature increases are less

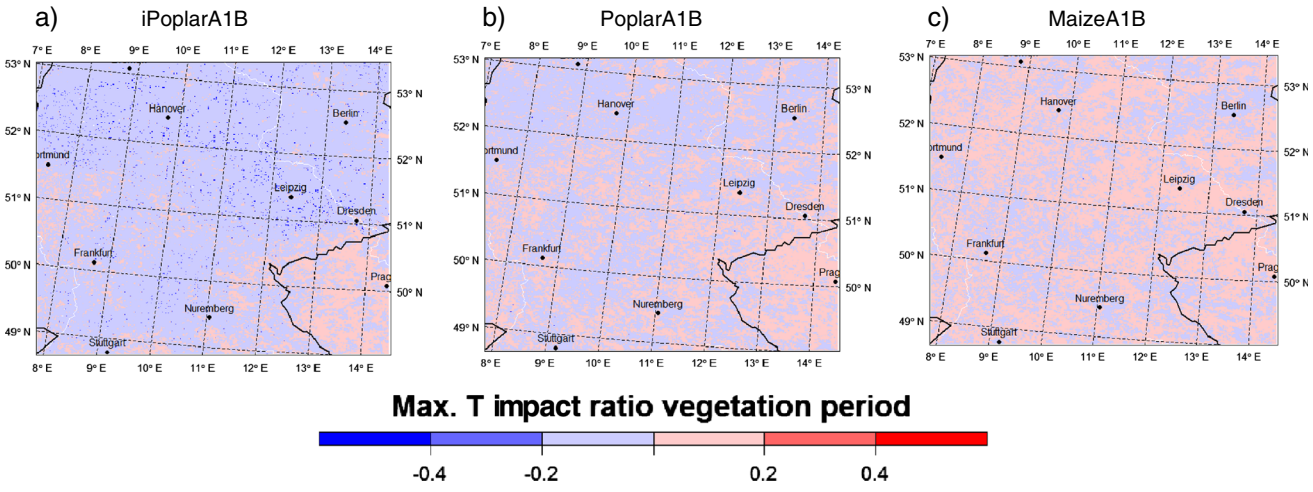

Figure 5. Impact ratio of maximum temperature during the vegetation period for (a) irrigated poplar, (b) nonirrigated poplar, and (c) maize.

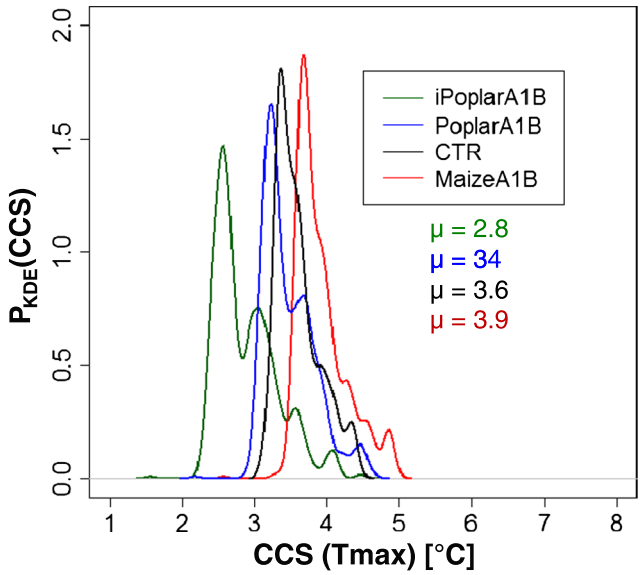

Figure 6. Probability distribution based on kernel density estimation of the climate change signal in maximum temperature of the reference simulation and the experiments which are significantly different from the control at 0.05 level based on bootstrap test. Difference of maximum temperature between 2071–2075 and 1971–1975.

pronounced in the case of the experiments with poplar and significantly different from the reference case (5% significance level, bootstrap test). The mean difference in percent of the vegetation scenarios in comparison to the control case and its standard deviation is presented in Figure 7. Extreme temperatures are estimated to be reduced by up to 20% for irrigated poplar and up to 5% for nonirrigated poplar (Figure 7). Changes in maximum temperature for maize are slightly increased compared to the reference case.

4.4. Local Versus Regional Projected Effects of Vegetation Change

To put the identified changes into perspective, we compare the local and regional climatic changes of the projected reference simulation with our projected vegetation scenario results. Such a comparison is useful because it helps to quantify the contribution of anthropogenic land cover change to projected climate trends on local and regional scales. Figures 8 and 9 show the extent and magnitude of the changes which are seen in seasonal cycles of many variables of the three vegetation scenarios (irrigated and nonirrigated poplar and maize) compared to the reference over local and regional scales for Central Germany, respectively. Hereby, the data are spatially and temporally averaged over the 5 years for each month of the year. We evaluate local effects by averaging the values of all bioenergy fields (red cells as in Figure 2). Regional effects are expressed by averaging over all nonbioenergy fields. Decreases in maximum temperatures of order 1°C in the case of poplar are generally accompanied by significant increases in latent heat fluxes (order of 45 W m^{-2}) and decreases in sensible heat fluxes (order of 40 W m^{-2}) on local scale during summer. The magnitude of change is even stronger for irrigated poplar than for nonirrigated poplar. A strong local increase in precipitation occurs when evapotranspiration is at its maximum in July. Although we see substantial

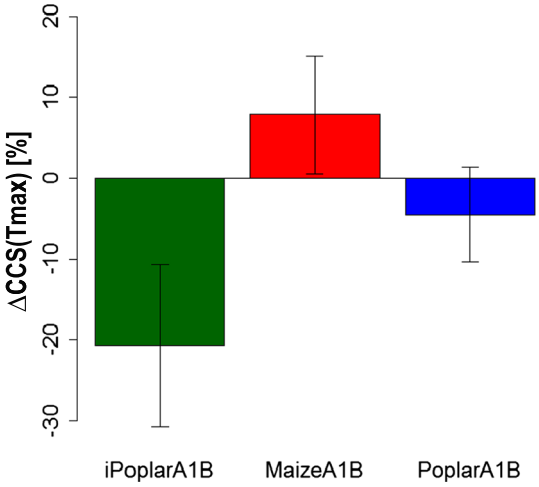

Figure 7. Mean difference in percent of the climate change signal of irrigated (green), nonirrigated poplar (blue), and maize (red) in comparison to the reference simulation as a bar plot and their associated standard deviation.

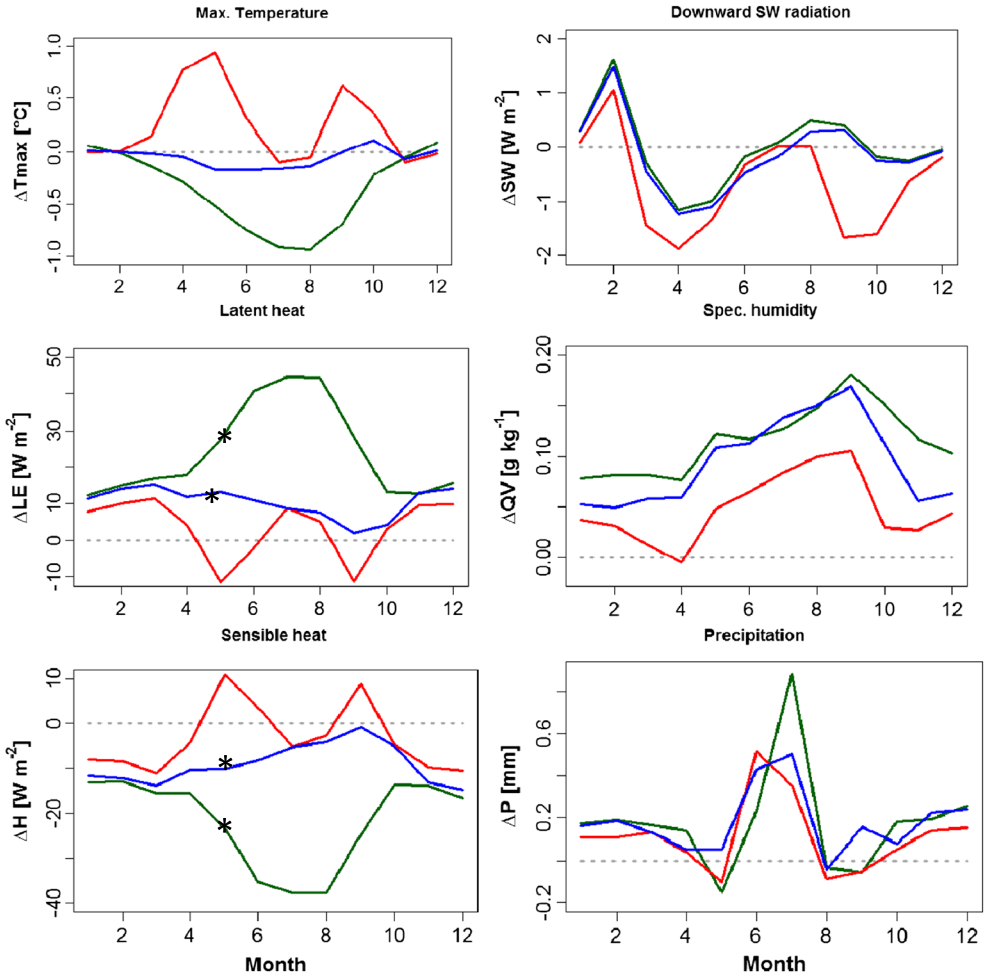

Figure 8. Local projected effects of vegetation change due to irrigated (green) and nonirrigated (blue) poplar and maize (red). Seasonal cycles of maximum temperature, latent heat and sensible heat flux, downward shortwave radiation, specific humidity, and precipitation. The data are spatially (bioenergy areas) and temporally (2071–2075) averaged for each month of the years. Stars denote significance at 0.05 level based on *U* test for the whole 12 months line. Note the different scale compared to Figure 10.

changes from a local perspective with modified land use, the prescribed alterations to surface vegetation cover lead not to large changes in the other regions without these specific land use changes (see regional effect in Figure 9). It is suggested that regional averages lack of sensitivity in response to land surface perturbations. The importance of the seasonal climate transitions in spring and fall due to agricultural practices (start of sowing and cropping) becomes evident in the maize scenario. During the onset of the growing season, when the LAI of maize is still at its minimum (April and May) compared to the reference, the temperature increases in the order of 1°C. The evaporative cooling effect starts in June after leaf emergence peaking in July with a cooling of similar magnitude. Cropping in September leads to a second minimum of LAI resulting in half of the warming in springtime.

Evidence of changes of many of the physical processes due to irrigated poplar compared to the reference and changes in the interactions are depicted by the correlation circle (see Figures 10a and 10b for local and regional changes based on principal component analysis as described in *Schlüter et al.* [2008]). The correlations among the variables along the first principal component are the most interesting ones. We have an anticorrelation between maximum temperature and latent heat and a positive correlation between maximum temperature and sensible heat meaning that as maximum temperatures decrease also sensible heat fluxes decrease and latent heat fluxes increase. However, absorbed shortwave radiation increases while maximum temperatures decrease in the local case. It is suggested

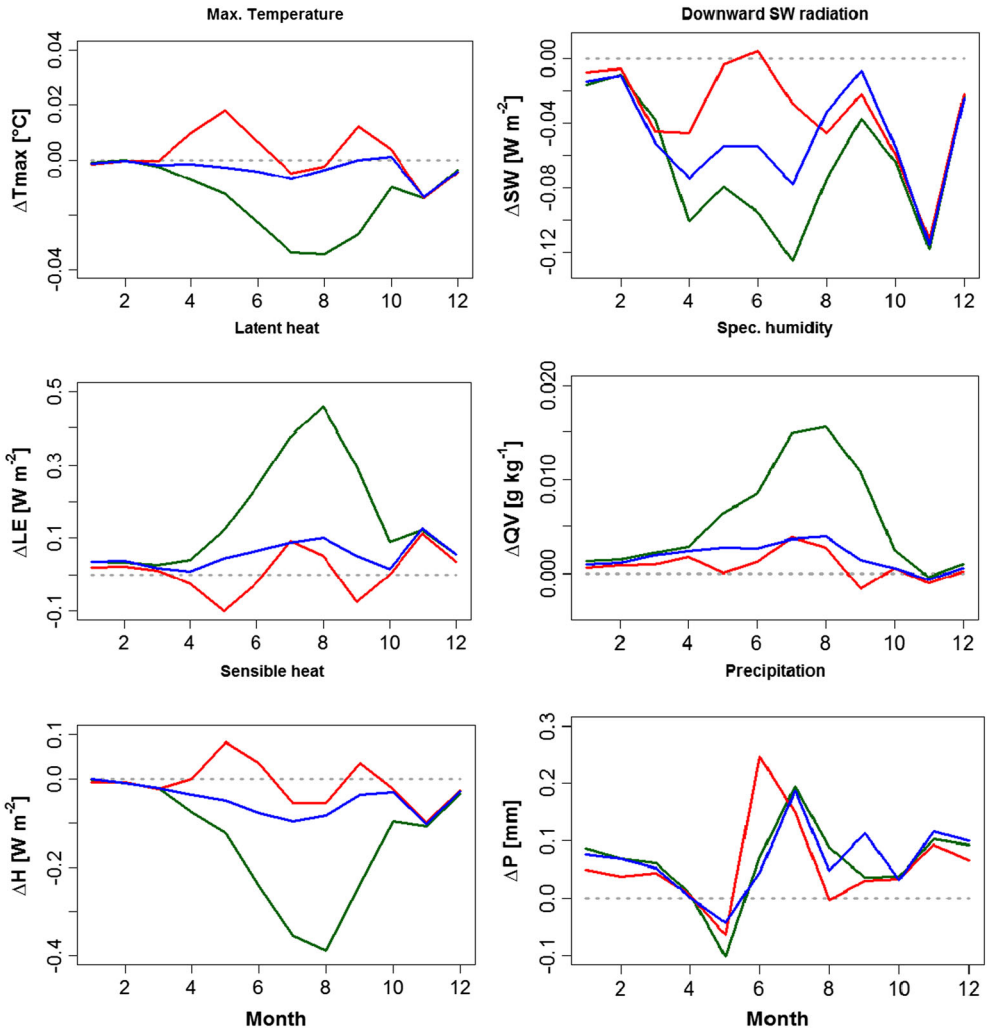

Figure 9. Regional projected effects of vegetation change due to irrigated (green) and nonirrigated (blue) poplar and maize (red). Seasonal cycles of maximum temperature, latent heat and sensible heat fluxes, downward shortwave radiation, specific humidity, and precipitation. The data are spatially (nonbioenergy areas) and temporally (2071–2075) averaged for each month of the years. Note the different scale compared to Figure 9.

that the evapotranspiration temperature influence is dominating over the radiation temperature influence. During the vegetation period the plant cover is increased compared to the reference case. An accompanying less reflective surface means that more incoming shortwave radiation is absorbed by the surface, making more energy available for sensible and latent heating. Although, if evapotranspiration is increased, less energy is available for sensible heat and the temperature decreases. The increase in absorbed shortwave radiation resulting from the changes in surface albedo is opposed by a regional decrease in surface shortwave radiation. This regional decrease may be accompanied by an increase in cloud cover resulting from increased moisture content of the near-surface atmosphere. It is suggested that the cloud effect dominates the shortwave radiation balance regionally, whereas the surface albedo effect dominates locally.

4.5. Local Projected Changes of Latent and Sensible Heat Due to Vegetation Change

The local projected changes in latent and sensible heat due to vegetation changes compared to the projected reference during the vegetation period are shown in Figures 11a and 11b. The figures show the probability function based on kernel density estimation of the future CCS (FCCS). The FCCS is the difference between the projected energy flux of each bioenergy plant averaged over the future period (2071–2075) and the projected energy flux (2071–2075) of the projected reference simulation for each

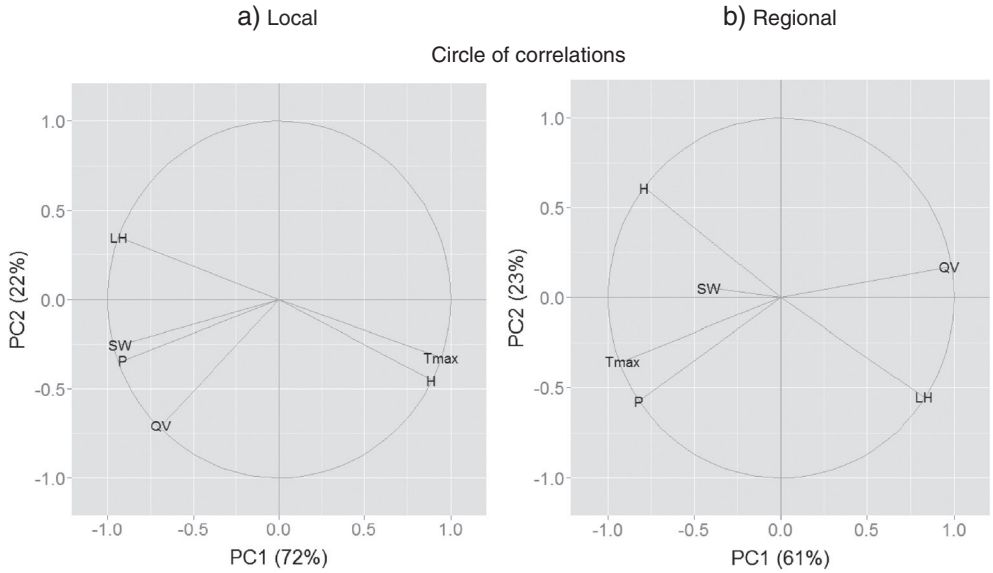

Figure 10. Correlation analysis based on principal component analysis on (a) local and (b) regional changes of vegetation period time series of irrigated poplar relative to the projected reference for maximum temperature, latent heat and sensible heat fluxes, downward shortwave radiation, specific humidity, and precipitation.

grid cell. Pronounced increases in latent heat fluxes are evident for irrigated poplar. Sensible heat fluxes decrease but to a minor degree. These changes affect the surface energy balance and thus the height of the boundary layer. Assuming a simplified energy balance by neglecting ground heat fluxes, the changed partition of latent heat and sensible heat fluxes during the vegetation period leads to a changed sum of those fluxes and with that to an average net increase of radiation of 5 W m^{-2} for irrigated poplar and of 2.7 W m^{-2} for nonirrigated poplar. The changes in the fluxes for maize are negative as well as positive during the vegetation period due to agricultural practices. Therefore, the overall net change of radiation is less pronounced.

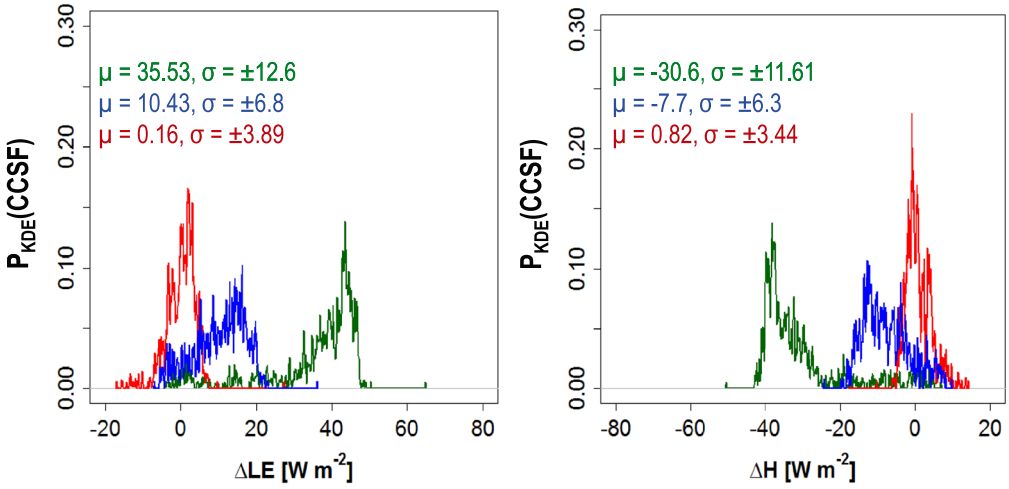

Figure 11. Probability distribution of local projected changes in partitioning of (a) latent and (b) sensible heat due to vegetation changes compared to the projected reference during the vegetation period, significantly different from the control at 0.05 level based on bootstrap test.

5. Discussion and Conclusions

The impact of increasing bioenergy production on arable land on the regional and local climate is shown as a case study for Germany having a temperate climate. The analysis includes the effect of irrigation as well as agricultural practices (start of sowing and cropping).

The range of extreme land use transformations for present climate demonstrates the applicability of the regional climate models for such studies. However, we show that the land-atmosphere response is nonlinear with linear land use change. In addition, downscaling to high resolutions (1.3 km in this study) is adding information to such climate simulations [see also *Tölle*, 2013]. This improves the accuracy of climate projections on the regional and in particular on the local scale by better representation of the land surface heterogeneity and orography and of explicit-resolving deep convection [*Prein et al.*, 2013; *Tölle*, 2013].

The extent and magnitude of a fictive but realistic land use transformation effect on local and regional future climate due to different forms of bioenergy plants such as irrigated, nonirrigated poplar, and maize are quantified for maximum temperature and the energy fluxes. The bioenergy plants are equally increased by 10% over the arable land of each federal state of Germany. By calculating the climate change signal between the years 1971–1975 and 2071–2075, we found a warming signal in Germany [*IPCC*, 2007; *Jacob et al.*, 2012]. Although the climate change signal reduces considerably with changes in land cover (in the case of poplar) compared to the reference signal, this is due to the higher albedo and increased evapotranspiration from rapid-growing poplar plantations which are cooling and moistening the climate during the vegetation period.

The changes are found to be largest locally for irrigated hybrid poplar, for which maximum temperatures declined by 1°C in summer months and specific humidity increased by 0.15 g kg^{-1}. The increased evapotranspiration during the vegetation period, which enhances the potential for moist deep convection, is likely to result in more precipitation (here 0.9 mm increase in July) as *Raddatz* [1998] suggested. The increase of surface radiative fluxes R_{net} due to changes in latent and sensible heat is estimated by 5 W m^{-2} on a local scale. Moreover, our results suggest that increases in the surface latent heat flux cause strong local evaporative cooling in the summer months [see also *Galos et al.*, 2013], whereas the associated regional cooling effect is also pronounced by increases in cloud cover, which alter the shortwave or longwave radiative fluxes and changes in atmospheric water vapor [*Pielke et al.*, 2007]. *Ban-Weiss et al.* [2011] found a decrease in global mean surface air temperature of 0.54°C by increasing the latent heat flux in an indealized study. In our study, we calculated a lower level of regional mean temperature changes. The strong local evaporation temperature influence may be offset by condensation of this water vapor in the atmosphere on a regional scale. Thus, increasing bioenergy production on arable land may result in local temperature changes but is not expected to cause substantial regional climate change in Germany.

One important aspect of our analysis is the impact of changes in agricultural practices which becomes evident in the maize case. While maize cools the near-surface boundary layer during its growing time by similar magnitude as for irrigated poplar, the late leaf unfolding time in May and cropping in September lead to a warming compared to the reference simulation. This shows the importance of climate transitions in spring and fall due to agricultural practices which is coupled to the vegetation phenology [*Levis et al.*, 2012; *Betts et al.*, 2013]. It is therefore likely that changes in vegetation types modify the future climate in Germany, potentially moderating extreme temperature increases in summer locally. The case of maize demonstrates the model sensitivity to its vegetation parameters especially to evapotranspiration and albedo which claims for a more accurate representation of those variables in regional climate models.

An open question remains how biochemical processes influence these results. On the one hand, hybrid poplar trees emit substantial amounts of volatile organic compounds; on the other hand, they can fix a large quantity of CO_2 due to their high growth rates. Future studies may therefore include those processes to improve the results.

Longer-term high-resolution simulations with additional vegetation scenarios are needed to confirm these results and explore the range in magnitude of land use changes. However, carrying out long-term simulations on such a scale is challenging in a reasonable time due to enormous computer power requirements.

It is recommended to use high-resolution climate simulations to account for future local-scale interactions between surface and boundary layer exchange processes. A two-way feedback regional climate model

would enable the impact analysis to the large-scale circulation. These results have wider implications for other regions such as regions susceptible to drought in Russia or the Great Plains in the U.S.

Acknowledgments
The work presented in this study was founded by the German Federal Ministry of Education and Research (BMBF) and is part of the BEST Research Framework (http://www.best-forschung.de). We also thank the German Weather Service (DWD) for providing the observational data. Computational resources were made available by the German Climate Computing Center (DKRZ) through support from the German Federal Ministry of Education and Research (BMBF).

References

Ament, F., and C. Simmer (2006), Improved representation of land-surface heterogeneity in a non-hydrostatic numerical weather prediction model, *Boundary Layer Meteorol.*, *121*(1), 153–174.

Anderson, C. J., P. Anex, and R. W. Arritt (2013), Regional climate impacts of a biofuels policy projection, *Geophys. Res. Lett.*, *40*, 1217–1222, doi:10.1002/grl.50179.

Ban-Weiss, G. A., G. Bala, L. Cao, J. Pongratz, and K. Caldeira (2011), Climate forcing and response to idealized changes in surface latent and sensible heat, *Environ. Res. Lett.*, *6*, 034032.

BEST (2011), Bioenergie-regionen stärken, http://best-forschung.uni-goettingen.de/.

Betts, A., R. Desjardins, D. Worth, and D. Cerkowniak (2013), Impact of land use change on the diurnal cycle climate of the Canadian Prairies, *J. Geophys. Res. Atmos.*, *118*, 11,996–12,011, doi:10.1002/2013JD020717.

Bonan, G. B. (2001), Observational evidence for reduction of daily maximum temperature by croplands in the Midwest United States, *J. Clim.*, *14*, 2430–2442.

Boucher, O., G. Myhre, and A. Myhre (2004), Direct human influence of irrigation on atmospheric water vapour and climate, *Clim. Dyn.*, *22*(6–7), 597–603.

Busch, G. (2012), GIS-based tools for regional assessments and planning processes regarding potential environmental effects of poplar SRC, *BioEnergy Res.*, *5*(3), 584–605.

Champeaux, J. L., V. Masson, and F. Chauvin (2005), ECOCLIMAP: A global database of land surface parameters at 1 km resolution, *Meteorol. Appl.*, *12*, 29–32, doi:10.1017/S1350482705001519.

Coumou, D., and A. Robinson (2013), Historic and future increase in the global land area affected by monthly heat extremes, *Environ. Res. Lett.*, *8*, 034018.

Dickinson, R. E., A. Henderson-Sellers, and P. J. Kennedy (1993), Biosphere-atmosphere transfer scheme (BATS) for the NCAR community climate model, *Tech. Rep.,* NCAR Technical Note, NCAR/TN-275+STR, 72 pp.

Doms, G., J. Förstner, E. Heise, H.-J. Herzog, M. Raschendorfer, R. Schrodin, R. Reinhardt, and G. Vogel (2005), A description of the nonhydrostatic regional model LM. Part 2: Physical parameterization, *Tech. Rep.,* DeutscherWetterdienst, Postfach 100465, 63007 Offenbach, Germany: Deutscher Wetterdienst, Offenbach.

Douville, H., S. Planton, J.-F. Royer, D. B. Stephenson, S. Tyteca, L. Kergoat, S. Lafont, and R. A. Betts (2000), Importance of vegetation feedbacks in doubled-CO2 climate experiments, *J. Geophys. Res.*, *105*(D11), 14,841–14,861.

EU (2009), *Directive 2009/28/EC of the European Parliament and of the Council of 23 April 2009 on the Promotion of the Use of Energy from Renewable Sources and Amending and Subsequently Repealing Directives 2001/77/EC and 2003/30/EC*, O. J. o. t. E. Union, EU, Brussels.

Farr, T. G., P. A. Rosen, E. Caro, R. Crippen, R. Duren, S. Hensley, and D. Alsdorf (2007), The shuttle radar topography mission, *Rev. Geophys.*, *45*, RG2004, doi:10.1029/2005RG000183.

Feddema, J. J. (2005), The importance of land-cover change in simulating future climates, *Science*, *310*, 1674–1678, doi:10.1126/science.1118160.

Galos, B., S. Hagemann, A. Hänsler, G. Kindermann, D. Rechid, K. Sieck, C. Teichmann, and D. Jacob (2013), Case study for the assessment of the biogeophysical effects of a potential afforestation in Europe, *Carbon Balance Manage.*, *8*(3), 1–12.

Gedney, N., and P. Valdes (2000), The effect of Amazonian deforestation on the Northern Hemisphere circulation and climate, *Geophys. Res. Lett.*, *27*(19), 3053–3056.

Georgescu, M., D. B. Lobell, and C. B. Field (2011), Direct climate effects of perennial biofuel crops in the United States, *Proc. Nat. Acad. Sci.*, doi:10.1073/pnas.1008779108.

Hollweg, H. J., et al. (2008), Ensemble simulations over Europe with the regional climate model CLM forced with IPCC AR4 global scenarios, *Tech. Rep. 3,* Model and Data Group at the Max Planck Institute for Meteorology, Hamb.

IPCC (2007), *Emission Scenarios*, Cambridge Univ. Press, Cambridge, U. K.

Jacob, D., K. Bülow, L. Kotova, C. Moseley, J. Petersen, and D. Recchid (2012), Regionale Klimaprojektionen für Europa und Deutschland: Ensemble-Simulationen für die Klimafolgenforschung, *CSC Rep. 6,* Climate Service Center.

Jones, A. D., W. D. Collins, and M. S. Torn (2013), On the additivity of radiative forcing between land use change and greenhouse gases, *Geophys. Res. Lett.*, *40*, 4036–4041, doi:10.1002/grl.50754.

Keil, M., M. Bock, T. Esch, A. Metz, S. Nieland, and A. Pfitzner (2011), Corine land cover aktualisierung 2006 für deutschland, *Tech. Rep.,* UBA-Texte | 13/2011, Berlin.

Knote, C., G. Heinemann, and B. Rockel (2010), Changes in weather extremes: Assessment of return values using high resolution climate simulations at convection-resolving scale, *Meteorol. Z.*, *19*(1), 11–23.

Levis, S., G. B. Bonan, E. Kluzek, P. E. Thornton, A. Jones, W. J. Sacks, and C. J. Kucharik (2012), Interactive crop management in the Community Earth System Model (CESM1): Seasonal influences on land-atmosphere fluxes, *J. Clim.*, *25*(14), 4839–4859, doi:10.1175/JCLI-D-11-00446.1.

Li, Z., and N. Mölders (2008), Interaction of impacts of doubling CO2 and changing regional land-cover on evaporation, precipitation, and runoff at global and regional scales, *Int. J. Climatol.*, *28*, 1653–1679, doi:10.1002/joc.1666.

Liedekerke, M. V., A. Jones, and P. Panagos (2006), *ESDBv2 Raster Library—A Set of Rasters Derived From the European Soil Database Distribution v2.0,* published by the European Commission and the European Soil Bureau Network, CD-ROM, EUR 19945 EN.

Lobell, D. B., and C. Bontils (2008), The effect of irrigation on regional temperatures: A spatial and temporal analysis of trends in California, *J. Clim.*, *21*(10), 2063–2071, doi:10.1175/2007JCLI1755.1.

Masson, V., J.-L. Champeaux, F. Chauvin, C. Meriguet, and R. Lacaze (2003), A global database of land surface parameters at 1-km resolution in meteorological and climate models, *J. Clim.*, *16*(9), 1261–1282.

Meehl, G. A., J. M. Arblaster, and C. Tebaldi (2005), Understanding future pattern of increased precipitation intensity in climate model simulations, *Geophys. Res. Lett.*, *32*, L18719, doi:10.1029/2005GL023680.

Monteith, J. L., and M. H. Unsworth (1990), *Principles of Environmental Physics*, Edward Arnold, London.

Müller-Westermaier (2004), Verfügbarkeit und qualität flächenbezogener klimadaten, *Tech. Rep.,* Deutscher Wetterdienst, Offenbach.

Nakicneovic, N., et al. (2000), *Emission Scenarios. A Special Report of Working Group III of the Intergovernmental Panel on Climate Change*, Cambridge Univ. Press, Cambridge, U. K.

Oleson, K. W., G. B. Bonan, S. Levis, and M. Vertenstein (2004), Effects of land use change on North American climate: Impact of surface datasets and model biogeophysics, *Clim. Dyn.*, *23*, 117–132, doi:10.1007/s00382-004-0426-9.

Özdemir, E. D., M. Härdtlein, and M. Eltrop (2009), Land substitution effects of biofuel side products and implications on the land area requirement for EU 2020 biofuel target, *Energy Policy*, *37*, 2986–2996.
Petzold, R., K.-H. Feger, and B. Siemer (2006), Standörtliche potenziale für den anbau schnellwachsender baumarten auf ackerflächen, *AFZ - Der Wald*, *16*, 855–857.
Petzold, R., K.-H. Feger, and H. Röhle (2010), *Standörtliche Voraussetzungen für Kurzumtriebplantagen*, pp. 44–53, AGROWOOD, Kurzumtriebsplantagen in Deutschland und europäische Perspektiven.
Pielke, R. A., J. Adegoke, A. Beltran-Przekurat, C. A. Hiemstra, J. Lin, U. S. Nair, D. Niyogi, and T. E. Nobis (2007), An overview of regional land-use and land-cover impacts on rainfall, *Tellus B*, *59*, 587–601.
Prein, A. F., A. Gobiet, M. Suklitsch, H. Truhetz, N. K. Awan, K. Keuler, and G. Georgievski (2013), Added value of convection permitting seasonal simulations, *Clim. Dyn.*, *41*(9–10), 2655–2677, doi:10.1007/s00382-013-1744-6.
Raddatz, R. L. (1998), Anthropogenic vegetation transformation and the potential for deep convection on the Canadian Prairies, *Can. J. Soil Sci.*, *78*, 657–666.
Ritter, B., and J. F. Geleyn (1992), A comprehensive radiation scheme for numerical weather prediction models with potential applications in climate simulations, *Mon. Weather Rev.*, *120*, 303–325.
Rockel, B., C. L. Castro, R. A. Pielke, H. vonStorch, and G. Leoncini (2008), Dynamical downscaling: Assessment of model system dependent retained and added variability for two different regional climate models, *J. Geophys. Res.*, *113*, D21107, doi:10.1029/2007JD009461.
Roeckner, E., R. Brokopf, M. Esch, M. Giorgetta, S. Hagemann, and L. Kornblueh (2006), Sensitivity of simulated climate to horizontal and vertical resolution in the ECHAM5 atmosphere model, *J. Clim.*, *19*, 3771–3791.
Röhricht, C., and K. Buscher (2009), Anbauempfehlungen Schnellwachsende Baumarten im Kurzumtrieb.
Sacks, W. J., B. I. Cook, N. Buenning, and S. Levis (2009), Effects of global irrigation on the near-surface climate, *Clim. Dyn.*, *33*(2–3), 159–175.
Schlüter, M. H., A. Merico, K. H. Wiltshire, W. Greve, and H. von Storch (2008), A statistical analysis of climate variability and ecosystem response in the German Bight, *Ocean Dyn.*, *58*(3–4), 169–186.
Scholz, V., B. Boelcke, F. Burger, M. Hofmann, and A. Vetter (2006), Produktion von pappeln und weiden auf landwirtschaftlichen flächen, *12 s*, Merkblatt KTBL - Datensammlung Energiepflanzen, Potsdam-Bornim.
Schrodin, R., and E. Heise (2002), The multi-layer version of the DWD soil model TERRA-LM, *COSMO Tech. Rep. 2,* Deutscher Wetterdienst, Offenbach.
Seneviratne, S. I., T. Corti, E. L. Davin, M. Hirschi, E. B. Jaeger, I. Lehner, B. Orlowsky, and A. J. Teuling (2010), Investigating soil moisture-climate interactions in a changing climate: A review, *Earth Sci. Rev.*, *99*, 125–161, doi:10.1016/j.earscirev.2010.02.004.
Smiatek, G., B. Rockel, and U. Schättler (2008), Time invariant data preprocessor for the climate version of the COSMO model (COSMO-CLM), *Meteorol. Z.*, *17*(4), 395–405.
Stegehuis, A. I., R. Vautard, P. Ciais, A. J. Teuling, M. Jung, and P. Yiou (2012), Summer temperatures in Europe and land heat fluxes in observation-based data and regional climate model simulations, *Clim. Dyn.*, *41*(2), 455–477, doi:10.1007/s00382-012-1559-x.
Swann, A. L., I. Y. Fung, and J. C. Chiang (2012), Mid-latitude afforestation shifts general circulation and tropical precipitation, *Proc. Nat. Acad. Sci.*, *109*(3), 712–716.
Tiedtke, M. (1989), A comprehensive mass flux scheme for cumulus parameterization in large scale models, *Mon. Weather Rev.*, *117*, 1779–1800.
Tölle, M. H. (2013), Less future warming and precipitation with fine scale resolution regional climate modelling, in Review.
Tölle, M. H., C. Moseley, O. Panferov, G. Busch, and A. Knohl (2013), Water supply patterns in two agricultural areas of Central Germany under climate change conditions, *Biogeosciences*, *10*, 2959–2972.
Turner, B. L., W. B. Meyer, and D. L. Skole (1994), Global land-use/land-cover change: Towards an integrated study, *Ambio*, *23*, 91–95.
Vanloocke, A., C. J. Bernacchi, and T. E. Twine (2010), The impacts of miscanthus x giganteus production on the Midwest US hydrological cycle, *Global Change Biol. Bioenergy*, *2*, 180–191, doi:10.1111/j.1757-1707.2010.01053.x.
Zaitchik, B. F., A. K. Macaldy, L. R. Bonneau, and R. B. Smith (2006), Europe's 2003 heat wave: A satellite view of impacts and land atmosphere feedbacks, *Int. J. Climatol.*, *26*, 743–769.